Comput Geosci (2017) 21:1313–1324
DOI 10.1007/s10596-017-9639-y

ORIGINAL PAPER

Numerical modeling of non-Newtonian fluid flow in fractures and porous media

Kai Bao[1] · Alexandre Lavrov[2] · Halvor Møll Nilsen[1]

Received: 30 September 2016 / Accepted: 10 March 2017 / Published online: 29 March 2017

Abstract Non-Newtonian fluids having Bingham or power-law rheology are common in many applications within drilling and reservoir engineering. Examples of such fluids are drilling muds, foams, heavy oil, hydraulic-fracturing and other stimulation fluids, and cement slurries. Despite the importance of non-Newtonian rheology, it is rarely used in reservoir simulators and fracture flow simulations. We study two types of non-Newtonian rheology: the truncated power-law (Ostwald-de Waele) fluid and the Bingham fluid. For either of the two types of non-Newtonian rheology, we construct relationships between the superficial fluid velocity and the pressure gradient in fractures and porous media. The Bingham fluid is regularized by means of Papanastasiou-type regularization for porous media and by means of a simple hyperbolic function for fracture flow. Approximation by Taylor expansion is used to evaluate the fluid velocity for small pressure gradients to reduce rounding errors. We report simulations of flow in rough-walled fractures for different rheologies and study the effect of fluid parameters on the flow channelization in rough-walled fractures. This effect is known from previous studies. We demonstrate how rheologies on different domains can be included in a fully-unstructured reservoir simulation that incorporates discrete fracture modeling (DFM). The above formulation was implemented in the open-source MATLAB Reservoir Simulation Toolbox (MRST), which uses fully implicit discretization on general polyhedral grids, including industry standard grids with DFM. This robust implementation is an important step towards hydro-mechanically coupled simulation of hydraulic fracturing with realistic non-Newtonian fluid rheology since most hydraulic fracturing models implemented so far make use of oversimplified rheological models (e.g., Newtonian or pure power-law).

Keywords Non-Newtonian fluid · Fracture · Porous media · Truncated power-law · Bingham fluid · MRST

✉ Kai Bao
Kai.Bao@sintef.no

Alexandre Lavrov
Alexandre.Lavrov@sintef.no

Halvor Møll Nilsen
HalvorMoll.Nilsen@sintef.no

[1] Mathematics and Cybernetics, SINTEF Digital, Oslo, Norway

[2] SINTEF Petroleum Research, Trondheim, Norway

1 Introduction

Non-Newtonian fluids are commonly encountered in oil-and-gas industry. Many fluids used in drilling, well cementing, and enhanced oil recovery have non-Newtonian rheology, e.g., water-based and non-aqueous drilling fluids, spacers, cement slurries, foams, hydraulic-fracturing fluids (including proppant-laden slurries), heavy oil, etc. In the simplest non-Newtonian model, the so-called generalized Newtonian model, the stress tensor is given by $\mathbf{T} = -P\mathbf{I}+2\mu_{\text{app}}\mathbf{D}$ where P is the fluid pressure, $\mathbf{I}$ is the identity tensor, μ_{app} is the apparent viscosity, and tensor $\mathbf{D}$ is the rate of deformation. The apparent viscosity is a function of the shear rate, $|\dot{\gamma}| = \sqrt{2\mathbf{D} : \mathbf{D}}$, in such fluids, unlike the Newtonian fluid where μ_{app} is a constant known as the dynamic viscosity, μ.

The difference between a Newtonian fluid and a non-Newtonian fluid can be illustrated by considering the shear stress vs. shear rate relationship in a simple shear flow [12]. This is the flow between two parallel walls being shifted

relative to each other. The flow is along the x-axis; the y-axis is normal to flow and normal to the walls. In such a flow, $\mathbf{D}$ is given by $\mathbf{D} = \frac{\dot{\gamma}}{2}\begin{pmatrix} 0 & 1 & 0 \\ 1 & 0 & 0 \\ 0 & 0 & 0 \end{pmatrix}$, thus the shear rate is given by $|\dot{\gamma}| = \sqrt{2\mathbf{D} : \mathbf{D}} = \frac{\partial u}{\partial y}$, where u is the fluid velocity. For a Newtonian fluid, such as water, the shear stress is directly proportional to the shear rate, with the coefficient of proportionality being the dynamic viscosity of the fluid (Fig. 1, solid line). Any other type of relationship between the shear stress and the shear rate indicates a non-Newtonian fluid. In order to predict the flow of such fluids in porous media as well as in natural or induced fractures, reservoir flow codes should incorporate non-Newtonian rheological models and closure laws.

Non-Newtonian fluids may have a zero or nonzero yield stress. When a fluid has a nonzero yield stress, a finite, nonzero shear stress must be applied in order for the fluid to start flowing. The simplest rheological model describing such a fluid is the Bingham model [34], in which the shear stress is a linear function of the shear rate, as illustrated by the dotted line in Fig. 1. The Bingham model is defined by two parameters: the yield stress, τ_Y, and the plastic viscosity μ_{pl}. In a simple shear flow, the shear stress *vs.* shear rate for such fluid is given by:

$$\tau = \tau_Y + \mu_{pl}|\dot{\gamma}| \tag{1}$$

Newtonian fluid can be regarded as a special case of the Bingham model, with $\tau_Y = 0$. Most fluids used for overbalanced drilling in oil-and-gas industry have yield stress. The yield stress is usually built by adding bentonite (a type of clay) or polymers to the drilling fluid. The purpose of having a yield stress in this case is to improve suspending properties of the drilling fluid: when the circulation is stopped (e.g., for tripping), the drilling fluid must be able to keep the drill cuttings in suspension. In a fluid without yield stress, solids would rapidly settle to the bottom-hole.

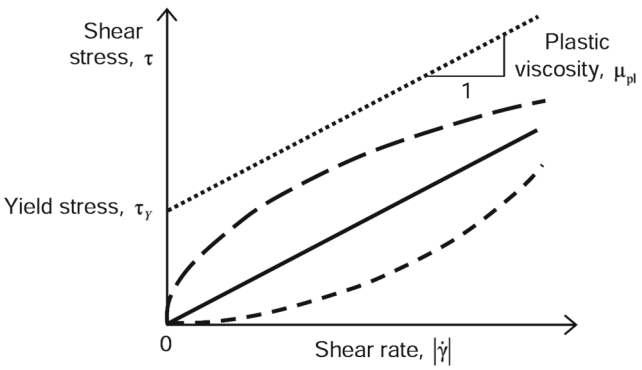

Fig. 1 Schematic plot of shear stress vs. shear rate for Newtonian (*solid line*) and non-Newtonian fluids in a simple shear flow. Non-Newtonian fluid with a yield stress is shown by the *dotted line*. Shear-thinning fluid without yield stress is shown by the *upper dashed line*. Shear-thickening fluid without yield stress is shown by the *lower dashed line*

A closed-form solution exists for Bingham fluid flow between parallel smooth walls ("a smooth-walled fracture"). The relationship between the fluid velocity averaged across the gap of the conduit, $\mathbf{u}$, and the pressure gradient, ∇P, is thereby given by [24, 25]:

$$\mathbf{u} = \begin{cases} 0 & \text{if } |\nabla P| \le \frac{2\tau_Y}{w} \\ \left[-\frac{w^2}{12\mu_{pl}} + \frac{w}{4\mu_{pl}}\frac{\tau_Y}{|\nabla P|} - \frac{1}{3w\mu_{pl}}\left(\frac{\tau_Y}{|\nabla P|}\right)^3\right]\nabla P & \text{if } |\nabla P| > \frac{2\tau_Y}{w} \end{cases}, \tag{2}$$

where w is the width of the conduit. A finite pressure gradient must therefore be applied in order to initiate the flow. The reason for this is that the fluid behaves like a solid if the shear stress is below the yield stress. Low shear stresses occur in the middle of the conduit. At the center plane of the smooth-walled conduit, the shear stress is zero. Thus, a solid, non-yielded plug exists near the center plane. The width of this plug is given by $\frac{2\tau_Y}{|\nabla P|}$. The width of the plug increases as the pressure gradient decreases, up until the plug occupies the entire width of the fracture when $|\nabla P| = \frac{2\tau_Y}{w}$. At this point, the flow stops. This introduces a discontinuity in the constitutive law and creates problems during numerical implementation of the Bingham rheology (or a yield-stress rheology, in general) in reservoir simulation. We will see later how this issue can be handled by introducing a regularization into the Bingham model.

Unlike flow in a fracture, there is no unique closed-form solution for Bingham fluid flow in porous media. A network model was employed by Bahlhoff et al. [4] to study flow of Bingham and other non-Newtonian fluids in porous media. Several numerical techniques (percolation, minimum threshold path, network and path of minimum pressure) were compared by Sochi [31]. A percolation-type model was used to analyze flow of a yield-stress fluid in porous media by Rossen and Gauglitz [28]. An ad-hoc relationship between the pressure gradient and the flow rate has been proposed in [35]. Scaling and simple relations could be obtained by means of, e.g., the homogenization theory. However, for real rocks, it seems more sensible to use experimental data and to adjust the ad-hoc model accordingly, as is done for permeabilities, relative permeabilities, and capillary pressure in traditional reservoir simulation. In this study, we will construct an *ad-hoc* functional relation for Bingham fluid flow in porous media (Eqs. 9 to 20 below) that captures the most essential features of such flow, in particular the existence of a threshold pressure gradient below which there is no flow.

For a Newtonian fluid ($\tau_Y = 0$), Eq. 2 turns into the textbook equation for Darcy flow in a smooth-walled conduit:

$$\mathbf{u} = -\frac{w^2}{12\mu}\nabla P \tag{3}$$

A non-Newtonian fluid without yield stress has a nonlinear shear stress vs. shear rate dependency. Such a fluid can be shear-thinning (Fig. 1, upper dashed line) or shear-thickening (Fig. 1, lower dashed line). For a shear-thinning fluid, the slope of shear stress vs. shear rate curve decreases with $|\dot{\gamma}|$. For a shear-thickening fluid, the slope increases with $|\dot{\gamma}|$. Many fracturing fluids are made shear-thinning by adding polymers. Shear-thinning rheology improves suspending properties of fracturing fluids, facilitating transport of proppant. The simplest rheological model used to describe a non-Newtonian fluid without yield stress is the power-law fluid defined by:

$$\tau = C|\dot{\gamma}|^n \tag{4}$$

where C is the consistency index; n is the flow behavior index. A shear-thinning fluid has $n < 1$; a shear-thickening fluid has $n > 1$. Newtonian fluid is a special case, obtained with $n = 1$. In the latter case, the consistency index is the dynamic viscosity of the Newtonian fluid.

Closed-form solution for the flow of a power-law fluid between two smooth parallel walls is given by:

$$u = -\frac{n}{2n+1}\frac{1}{C^{\frac{1}{n}}}\frac{1}{|\nabla P|^2}\left(\frac{w|\nabla P|}{2}\right)^{\frac{n+1}{n}}\nabla P \tag{5}$$

For a Newtonian fluid ($n = 1$, $C = \mu$), Eq. 5 turns into Eq. 3.

No unique closed-form solution is available for the flow of a power-law fluid in porous media. Shah and Yortsos [30] derived a closed-form solution using the homogenization theory for a periodic medium. They also provided an overview of other proposed expressions available by the time.

Equation 4 suggests that, for $n < 1$, the derivative $\frac{d\tau}{d\dot{\gamma}}$ becomes infinite as $\dot{\gamma} \to 0$ and $\lim_{\dot{\gamma}\to\infty}\left(\frac{d\tau}{d\dot{\gamma}}\right) \to 0$. This is unphysical since the differential viscosity, $|\frac{d\tau}{d\dot{\gamma}}|$, should be positive and finite, on physical grounds. Likewise, for $n > 1$, Eq. 4 yields zero differential viscosity at $\dot{\gamma} = 0$ and infinite differential viscosity as $\dot{\gamma} \to \infty$. To remediate these issues, more advanced rheological models have been introduced, e.g., the Carreau model [7, 8]. The main disadvantage of these models is that they do not permit a closed-form solution for laminar flow between two parallel plates.

In order to remediate the issue of zero and infinite viscosities pertaining to Eq. 4, a truncated power-law model has been introduced [5]. This fluid behaves like a power-law fluid within an intermediate range of shear rates, and like a Newtonian fluid at very high and very low flow rates. The differential viscosity is therefore always nonzero and finite. The shear stress vs. shear rate relationship for a truncated power-law model is given by:

$$\tau = \begin{cases} \mu_0\dot{\gamma} & \text{for } |\dot{\gamma}| \le \left(\frac{C}{\mu_0}\right)^{\frac{1}{n-1}} \\ C|\dot{\gamma}|^{n-1}\dot{\gamma} & \text{for } \left(\frac{C}{\mu_0}\right)^{\frac{1}{n-1}} < |\dot{\gamma}| \le \left(\frac{C}{\mu_\infty}\right)^{\frac{1}{n-1}} \\ \mu_\infty\dot{\gamma} & \text{for } |\dot{\gamma}| > \left(\frac{C}{\mu_\infty}\right)^{\frac{1}{n-1}} \end{cases} \tag{6}$$

where C is the consistency index, n is the flow behavior index, and μ_0 and μ_∞ are dynamic viscosities of the (Newtonian) fluid at low and high shear stress, respectively. The truncated power-law model has four free parameters, similarly to the Carreau model. However, unlike the Carreau model, it enables a closed form solution for the flow between two smooth parallel walls [19]:

$$\mathbf{u} = \begin{cases} -\frac{w^2}{12\mu_0}\nabla P & \text{if } |\nabla P| \le \frac{2\mu_0}{w}\left(\frac{C}{\mu_0}\right)^{\frac{1}{1-n}} \\ -\left[\frac{2}{3}\cdot\frac{1-n}{1+2n}\cdot\frac{C^{\frac{3}{1-n}}}{\mu_0^{\frac{1+2n}{1-n}}|\nabla P|^3 w} + \frac{2n}{1+2n}\cdot\frac{\left(\frac{w}{2}\right)^{\frac{1+2n}{n}}}{wC^{\frac{1}{n}}}|\nabla P|^{\frac{1-n}{n}}\right]\nabla P & \text{if } \frac{2\mu_0}{w}\left(\frac{C}{\mu_0}\right)^{\frac{1}{1-n}} < |\nabla P| \le \frac{2\mu_\infty}{w}\left(\frac{C}{\mu_\infty}\right)^{\frac{1}{1-n}} \\ -\left[\frac{w^2}{12\mu_\infty} - \frac{2}{3}\cdot\frac{1-n}{1+2n}\cdot\frac{C^{\frac{3}{1-n}}}{|\nabla P|^3 w}\left(\frac{1}{\mu_\infty^{\frac{1+2n}{1-n}}} - \frac{1}{\mu_0^{\frac{1+2n}{1-n}}}\right)\right]\nabla P & \text{if } \frac{2\mu_\infty}{w}\left(\frac{C}{\mu_\infty}\right)^{\frac{1}{1-n}} < |\nabla P| \end{cases} \tag{7}$$

where w is the aperture size. The truncated power-law model can be used to represent the rheology of hydraulic fracturing fluids (gels). There have been no attempts to apply the truncated power-law rheology for flow in porous media.

As with the Bingham fluid, there is no unique closed-form "flow rate vs. pressure gradient" relationship for the flow of a truncated power-law fluid in porous media. Deriving such solution could be attempted by using, e.g., the homogenization theory. However, the result would not

be unique, and the model still would need to be calibrated via experiments. It seems therefore more sensible to construct an *ad-hoc* model and then to use experimental data in order to adjust the model. In this study, we will construct an *ad-hoc* functional relation for truncated power-law fluid flow in porous media (Eqs. 27 to 29 below) that captures the most essential features of the flow. In particular, the flow reduces to a Newtonian fluid flow at very high and very low superficial fluid velocities.

Non-Newtonian rheology needs to be properly taken into account when modeling flow in porous media and in fractures. For instance, nonzero yield stress of drilling fluids prevents them from entering pores and fractures before the applied pressure gradient exceeds a certain threshold value. Therefore, in order to construct reliable numerical models of mud losses and extended leak-off test, the flow equations must be closed with a rheological model that includes yield stress [20]. Moreover, when a shear-thinning fluid or a yield stress fluid flows in a rough-walled fracture, "dead zones" can develop where there is no flow. This affects the effective permeability of the fracture to such fluids [16]. It also affects transport since the flow becomes more channelized [2, 3, 17, 18]. In hydraulic fracturing models, power-law rheology has been routinely used to describe fracturing gels [27, 33].

A word of caution is due with regard to the use of Eqs. 2, 3, 5, and 7 for flow in rock fractures. Unlike smooth-walled conduits, for which these equations have been derived, real fractures have rough walls. Asperities protruding from the fracture faces make the flow paths tortuous. It means that the same pressure difference is applied to a longer pathline in the fracture plane. This effectively reduces the fracture permeability as compared to that of a smooth-walled fracture of the same average aperture. Therefore, the average aperture of a rough-walled fracture, i.e., the mean separation of the fracture faces, is a poor indicator of the fracture flow resistance. Instead, the hydraulic aperture should be used. The hydraulic aperture, w_h, is the aperture of a smooth-walled fracture that yields the same flow rate at a given pressure differential as the rough-walled fracture [6, 15, 36]. The Newtonian-fluid velocity in a rough-walled fracture is then given by:

$$\mathbf{u} = -\frac{w_\mathrm{h}^2}{12\mu}\nabla P \tag{8}$$

Roughness cannot be modeled explicitly in a reservoir simulator since its geometric scale is too small (to make things even more complicated, there is a hierarchy of roughnesses and the fracture landscape is usually a fractal surface, with the Hurst exponent of 0.7...0.8). This should be kept in mind when applying Eqs. 2, 3, 5, and 7 in reservoir simulation. The fracture aperture, w, is therefore always understood as *hydraulic* rather than mechanical aperture in this article.

2 Implementation of Bingham model and truncated power-law model in reservoir simulation

Our objective in this study is to construct relationships between the flow rate (or, equivalently, the superficial fluid velocity) and the pressure gradient for single-phase flow in porous media and in fractures, to be used in hydraulic fracturing and reservoir flow simulations. Fractures can thereby be represented as collections of elements (tetrahedra in 3D) with increased permeability. The fracture permeability depends on the fracture opening. Representing a fracture as a collection of failed elements (gridblocks) is a viable approach and has been used, e.g., in fully-3D hydraulic fracturing models [1, 21, 22].

In this artaicle, we focus on the implementation of the Bingham model and the truncated power-law model in the MATLAB Reservoir Simulation Toolbox (MRST) [23]. Discrete fracture model [13, 29] is employed to represent the fractures and handle the flow between fractures and porous media.

2.1 Bingham model for porous media flow

An *ad-hoc* analogue of Darcy's law can be constructed for Bingham fluid flow in porous media as follows. The essential feature of the Bingham fluid is the threshold value of the pressure gradient below which there is no flow. The threshold pressure gradient must be an increasing function of the yield stress, τ_Y. The simplest model that satisfies these requirements is given by [35]:

$$\mathbf{u} = \begin{cases} 0 & \text{if } |\nabla P| \le \frac{\tau_\mathrm{Y}}{d} \\ -M\nabla P & \text{if } |\nabla P| > \frac{\tau_\mathrm{Y}}{d} \end{cases}, \tag{9}$$

where ∇P is the pressure gradient between two gridblocks, M is the fluid mobility between the gridblocks, and d is a material parameter of the porous media, namely a characteristic internal length. The value of d is on the order of the pore throat diameter. It is well known that the threshold pressure gradient required to initiate flow of a yield-stress fluid in porous media depends on the details of the porous structure (e.g., [31]). Therefore, it is, in general, not possible to cover all the complexity of yield-stress fluid flow in porous media only with a single structural parameter, d. Nevertheless, we use this oversimplified approach here as a first-order approximation. For a detailed discussion of the yield-stress issue in porous media the reader is referred to [31]. The mobility can be represented e.g. as the harmonic average of the mobility values in the two gridblocks:

$$M = \frac{2M_1M_2}{M_1 + M_2} \tag{10}$$

with the mobility of gridblock i defined as follows [35]:

$$M_{\mathrm{i}} = \frac{k_{\mathrm{i}}}{\mu_{\mathrm{pl}}}\left(1 - \frac{\tau_{\mathrm{Y}}}{d|\nabla P|}\right) \tag{11}$$

where k_{i} is the absolute permeability of the ith gridblock to Newtonian fluid.

Implementation of the Bingham model according to Eqs. 9 to 11 leads to instabilities and convergence problems since it involves a discontinuity in the flow rate *vs.* pressure gradient. A common remedy is regularization of the Bingham model. Several types of regularization have been proposed in computational rheology. The most popular one is probably the Papanastasiou regularization [26]. A thorough comparative study carried out by Frigaard and Nouar [10] revealed that the Papanastasiou regularization performs better than other types of regularization in computational fluid dynamics of Bingham fluids. The Papanastasiou regularization of Eq. 1 is given by:

$$\tau = \tau_{\mathrm{Y}}[1 - exp(-m|\dot{\gamma}|)] + \mu_{\mathrm{pl}}|\dot{\gamma}| \tag{12}$$

where m is a regularization parameter. As evident from Fig. 2, the regularization removes the singularity and makes the shear rate nonzero everywhere.

Introducing the non-dimensional shear rate, the non-dimensional shear stress, the non-dimensional apparent viscosity, and the non-dimensional regularization parameter as follows:

$$\begin{cases} |\tilde{\dot{\gamma}}| &= \frac{|\dot{\gamma}|\mu_{\mathrm{pl}}}{\tau_{\mathrm{Y}}} \\ \tilde{\tau} &= \frac{\tau}{\tau_{\mathrm{Y}}} \\ \tilde{\mu}_{\mathrm{app}} &= \frac{\mu_{\mathrm{app}}}{\mu_{\mathrm{pl}}} \\ \tilde{m} &= \frac{m\tau_{\mathrm{Y}}}{\mu_{\mathrm{pl}}} \end{cases}, \tag{13}$$

the Bingham model becomes:

$$\tilde{\mu}_{\mathrm{app}} = 1 + |\tilde{\dot{\gamma}}|^{-1} \tag{14}$$

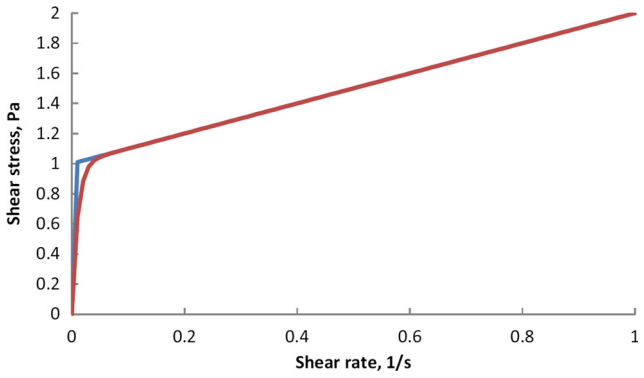

Fig. 2 An example of Papanastasiou regularization (*red*) of Bingham model (*blue*)

while the regularized Bingham model becomes:

$$\tilde{\mu}_{\mathrm{app}} = 1 + \frac{1 - exp(-\tilde{m}|\tilde{\dot{\gamma}}|)}{|\tilde{\dot{\gamma}}|} \tag{15}$$

It is evident from Eq. 15 that the regularized model approaches the "true" Bingham model as $\tilde{m} \to \infty$.

The following relationship between the pressure gradient, $|\nabla P|$, and the superficial fluid velocity, $\mathbf{u}$, in porous media can then be constructed in order to regularize the "true" Bingham model:

$$\mathbf{u} = -\frac{\nabla P}{|\nabla P|}u \tag{16}$$

where $u = |\mathbf{u}|$ is the magnitude of the superficial fluid velocity, to be obtained from the following nonlinear equation:

$$\frac{|\nabla P|d}{\tau_{\mathrm{Y}}} = 1 + \frac{\mu_{\mathrm{pl}}d}{k\tau_{\mathrm{Y}}}u - exp\left(-\frac{\tilde{m}\mu_{\mathrm{pl}}d}{k\tau_{\mathrm{Y}}}u\right) \quad \text{for all } |\nabla P| \tag{17}$$

where k is the permeability of the porous media (harmonic average of the absolute permeabilities of the two gridblocks, $k = \frac{2k_1k_2}{k_1+k_2}$), d is the characteristic internal length scale of the porous media as defined above, and $\tilde{m}$ is a non-dimensional regularization parameter defined as follows:

$$\tilde{m} = \frac{m\tau_{\mathrm{Y}}}{\mu_{\mathrm{pl}}} \tag{18}$$

Introducing the dimensionless pressure gradient and the dimensionless superficial fluid velocity as follows:

$$\begin{aligned} |\nabla\tilde{P}| &= |\nabla P|\frac{d}{\tau_{\mathrm{Y}}} \\ \tilde{u} &= u\frac{\mu_{\mathrm{pl}}d}{k\tau_{\mathrm{Y}}} \end{aligned} \tag{19}$$

leads to the following dimensionless from of Eq. 17:

$$|\nabla\tilde{P}| = 1 + \tilde{u} - exp(-\tilde{m}\tilde{u}) \tag{20}$$

Equation 20 is plotted in Fig. 3 for $\tilde{m} = 100$. Increasing $\tilde{m}$ improves the approximation of the original "true" Bingham model.

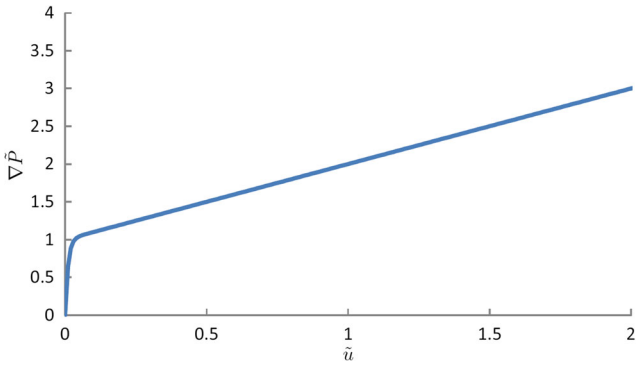

Fig. 3 Regularized Bingham model for flow in porous media, Eq. 20

2.2 Bingham model for fracture flow

Consider now flow in a fracture. In the reservoir simulator's framework, this is the flow between two "failed" ("fractured") gridblocks. Without regularization, the fluid velocity vs. pressure gradient dependency could be constructed, for example, by using Eq. 9 with the mobility defined as follows:

$$M = \begin{cases} 0 & \text{if } |\nabla P| \le \frac{2\tau_Y}{w} \\ \frac{w^2}{12\mu_{pl}} - \frac{w}{4\mu_{pl}}\frac{\tau_Y}{|\nabla P|} + \frac{1}{3w\mu_{pl}}\left(\frac{\tau_Y}{|\nabla P|}\right)^3 & \text{if } |\nabla P| > \frac{2\tau_Y}{w} \end{cases} \tag{21}$$

In Eq. 21, the average fracture aperture can be calculated as the harmonic average of the fracture apertures in gridblocks 1 and 2:

$$w = \frac{2w_1 w_2}{w_1 + w_2} \tag{22}$$

Convergence problems experienced with the "true" Bingham model [Eq. 21] motivates the use of a regularization for fracture flow as well. Introducing the dimensionless pressure gradient and the dimensionless superficial fluid velocity as follows:

$$\begin{aligned} |\nabla \tilde{P}| &= |\nabla P|\frac{w}{2\tau_Y} \\ \tilde{u} &= u\frac{\mu_{pl}}{w\tau_Y} \end{aligned} \tag{23}$$

the "true" Bingham model would be given by (cf. Eqs. 9 and 21):

$$\tilde{u} = \begin{cases} 0 & \text{if } |\nabla \tilde{P}| \le 1 \\ \frac{1}{6}|\nabla \tilde{P}| - \frac{1}{4} + \frac{1}{12}\frac{1}{|\nabla \tilde{P}|^2} & \text{if } |\nabla \tilde{P}| > 1 \end{cases} \tag{24}$$

Equation 24 can be regularized as follows:

$$\tilde{u} = \left[\left(\frac{1}{4}\right)^n + \left(\frac{1}{6}\right)^n |\nabla \tilde{P}|^n\right]^{\frac{1}{n}} - \frac{1}{4} \quad \text{for all } |\nabla \tilde{P}| \tag{25}$$

where n is a dimensionless regularization parameter.

At small pressure gradient values, Eq. 25 involves subtraction of two close values. This is not good for numerical implementation and can be remedied by Taylor expansion of the right-hand side of Eq. 25 for small $|\nabla \tilde{P}|$. Equation 25 then becomes:

$$\tilde{u} \approx \frac{1}{4n}\left(\frac{4|\nabla \tilde{P}|}{6}\right)^n \quad \text{for small } |\nabla \tilde{P}| \tag{26}$$

The values of n can be chosen within the range from 4 to 6 (Fig. 4).

The model of Bingham fluid flow in a fracture given by Eq. 21 is the classical and the simplest one, and has been used previously, e.g., in [11]. More elaborate models, taking into account the self-affinity of fracture landscape, have become available recently [32] and can be considered for implementation in future.

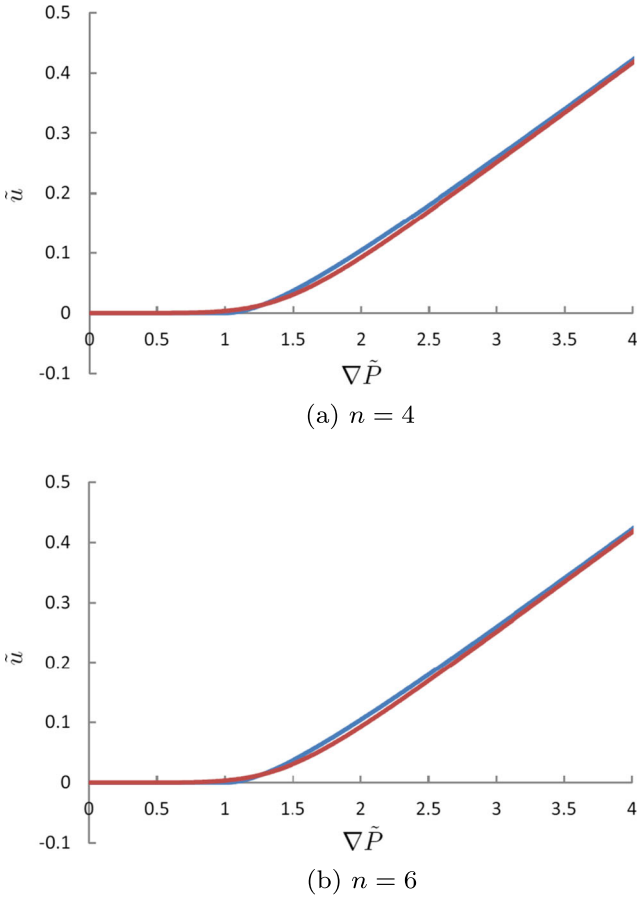

(a) $n = 4$

(b) $n = 6$

Fig. 4 Regularized Bingham model for fracture flow, with $n = 4$ (**a**) and $n = 6$ (**b**). *Blue curve*: "true" Bingham model given by Eq. 24. *Red curve*: regularized Bingham model given by Eq. 25

2.3 Bingham model for flow between a porous media element and a fracture element (leak-off)

This is effectively flow (leak-off) through the fracture wall or from the fracture tip into the porous media. The flow is dominated by the intact gridblock in this case since the flow in the fracture is mostly from failed gridblock to failed gridblock. Equation 17 or its non-dimensional counterpart, Eq. 20, are to be used in this case, with the permeability, k, being the permeability of the intact gridblock.

2.4 Truncated power-law model for porous media flow

An *ad-hoc* analogue of Darcy's law can be constructed for the truncated power-law fluid flow in porous media as follows. An essential feature of the truncated power-law fluid is that it approaches a Newtonian fluid at very high and very low shear rates. The simplest porous media flow model that has similar behavior is given by:

$$\mathbf{u} = -M\nabla P \quad \text{for all } |\nabla P| \tag{27}$$

with the mobility given by Eq. 10. The individual mobilities of gridblocks entering Eq. 10 can be defined as follows, in order to resemble the truncated power-law rheology:

$$M_{\mathrm{i}} = \begin{cases} \frac{k_{\mathrm{i}}}{\mu_0} & \text{if } |\nabla P| \le \epsilon_1 \\ \left(\frac{l_{\mathrm{i}}^{\frac{1+n}{n}}}{C^{\frac{1}{n}}} \right) |\nabla P|^{\frac{1-n}{n}} \tilde{k}_{\mathrm{i}} & \text{if } \epsilon_1 < |\nabla P| \le \epsilon_2 \\ \frac{k_{\mathrm{i}}}{\mu_\infty} & \text{if } \epsilon_2 < |\nabla P| \end{cases} \tag{28}$$

where $\epsilon_1 = \left(\frac{k_{\mathrm{i}}}{\tilde{k}_{\mathrm{i}}\mu_0}\right) \frac{C^{\frac{1}{1-n}}}{l_{\mathrm{i}}^{\frac{1+n}{1-n}}}$, $\epsilon_2 = \left(\frac{k_{\mathrm{i}}}{\tilde{k}_{\mathrm{i}}\mu_\infty}\right) \frac{C^{\frac{1}{1-n}}}{l_{\mathrm{i}}^{\frac{1+n}{1-n}}}$, where l_{i} is the characteristic internal length of the porous media in the ith gridblock and has the meaning of the "typical" pore throat size; $\tilde{k}_{\mathrm{i}}$ is a dimensionless parameter, specified for each gridblock. Parameters k_{i}, l_{i}, and $\tilde{k}_{\mathrm{i}}$ are not independent. The relationship between the three parameters becomes transparent if we consider a specific case of truncated power-law model, namely the Newtonian fluid. In this case, $\mu_0 = \mu_\infty = C$ should represent the dynamic viscosity, and Darcy's law must hold at all values of $|\nabla P|$. In particular, the second of Eqs. 28 should reduce to Darcy's law. This is only possible if the following relationship between k_{i}, l_{i} and $\tilde{k}_{\mathrm{i}}$ holds:

$$k_{\mathrm{i}} = \tilde{k}_{\mathrm{i}} l_{\mathrm{i}}^2 \tag{29}$$

The truncated power-law model for flow in porous media has thus six parameters (four for the fluid and two for each gridblock, incl. the absolute permeability).

2.5 Truncated power-law model for fracture flow

The superficial fluid velocity vs. pressure gradient is given by Eq. 27 in this case, with the mobility, M, given by Eq. 10. Individual mobilities of gridblocks entering Eq. 10 can be evaluated analytically from the closed-form fracture flow equations available for this rheology and given by the above Eq. 7 [19]:

$$M_{\mathrm{i}} = \begin{cases} \frac{w_{\mathrm{i}}^2}{12\mu_o} & \text{if } |\nabla P| \le \frac{2\mu_o}{w_{\mathrm{i}}} \left(\frac{C}{\mu_o}\right)^{\frac{1}{1-n}} \\ \frac{2}{3} \cdot \frac{1-n}{1+2n} \cdot \frac{C^{\frac{3}{1-n}}}{\mu_o^{\frac{1+2n}{1-n}} |\nabla P|^3 w_{\mathrm{i}}} + \frac{2n}{1+2n} \cdot \frac{\left(\frac{w_{\mathrm{i}}}{2}\right)^{\frac{1+2n}{n}}}{w_{\mathrm{i}} C^{\frac{1}{n}}} |\nabla P|^{\frac{1-n}{n}} & \text{if } \frac{2\mu_o}{w_{\mathrm{i}}} \left(\frac{C}{\mu_o}\right)^{\frac{1}{1-n}} < |\nabla P| \le \frac{2\mu_\infty}{w_{\mathrm{i}}} \left(\frac{C}{\mu_\infty}\right)^{\frac{1}{1-n}} \\ \frac{w_{\mathrm{i}}^2}{12\mu_\infty} - \frac{2}{3} \cdot \frac{1-n}{1+2n} \cdot \frac{C^{\frac{3}{1-n}}}{|\nabla P|^3 w_{\mathrm{i}}} \left(\frac{1}{\mu_\infty^{\frac{1+2n}{1-n}}} - \frac{1}{\mu_o^{\frac{1+2n}{1-n}}} \right) & \text{if } \frac{2\mu_\infty}{w_{\mathrm{i}}} \left(\frac{C}{\mu_\infty}\right)^{\frac{1}{1-n}} < |\nabla P| \end{cases} \tag{30}$$

Here, w_{i} is the aperture size.

2.6 Truncated power-law model for flow between a porous media element and a fracture element (leak-off)

This is effectively flow (leak-off) through the fracture wall or from the fracture tip into the porous media. The flow is dominated by the intact gridblock in this case since the flow in the fracture is mostly from failed gridblock to failed gridblock. Equation 27 is to be used in this case, with the mobility, M, referring to the intact gridblock and calculated using Eq. 28, where parameters, k_{i}, l_{i}, and $\tilde{k}_{\mathrm{i}}$, refer to the intact gridblock.

3 Examples

To demonstrate the application of the models developed above, we apply them to the flow of Bingham fluid and truncated power-law fluid in a rough-walled rectangular fracture. The distribution of the fracture aperture is shown in Fig. 5. The in-plane dimensions of the fracture are 65 cm × 65 cm. Two fractures were constructed: with the mean aperture equal to 1.7-mm and with the mean aperture equal to 1.02 mm. The former one had nonzero aperture everywhere; the latter had zero aperture (closed fracture) at some locations. The 1.7-mm fracture (Fig. 5) was produced

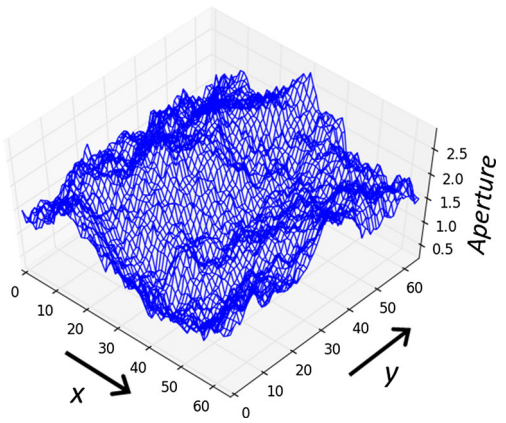

Fig. 5 Distribution of the fracture aperture (mm) in the fracture plane of the 1.7-mm fracture. The in-plane dimensions of the fracture: 65 cm × 65 cm

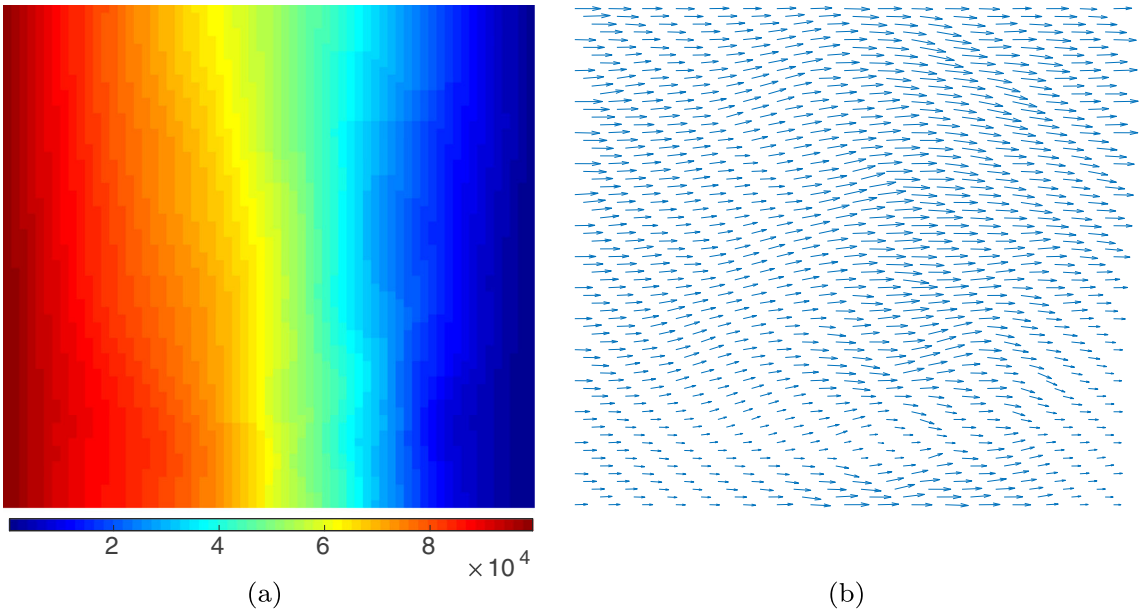

Fig. 6 Distribution of the fluid pressure (**a**) and superficial fluid velocity (**b**) in the 1.7-mm fracture. The fracture has nonzero aperture everywhere

numerically by generating two rough surfaces with the Hurst exponent equal to 0.7, placing the surfaces opposite to each other, and subtracting them. The 1.02-mm fracture was produced by subtracting 0.68 mm from the apertures of the 1.7-mm fracture.

In the simulations, the pressure gradient was applied along the x-axis, between two opposite sides of the fracture. The flow rate was calculated. Simulations were run for a wide range of pressure differentials. Based on the fluid velocity field obtained in the simulation, the tortuosity of the flow was calculated. Tortuosity was defined as follows [9, 14]:

$$T = \frac{\langle |\mathbf{u}| \rangle}{\langle u_{\parallel} \rangle}, \tag{31}$$

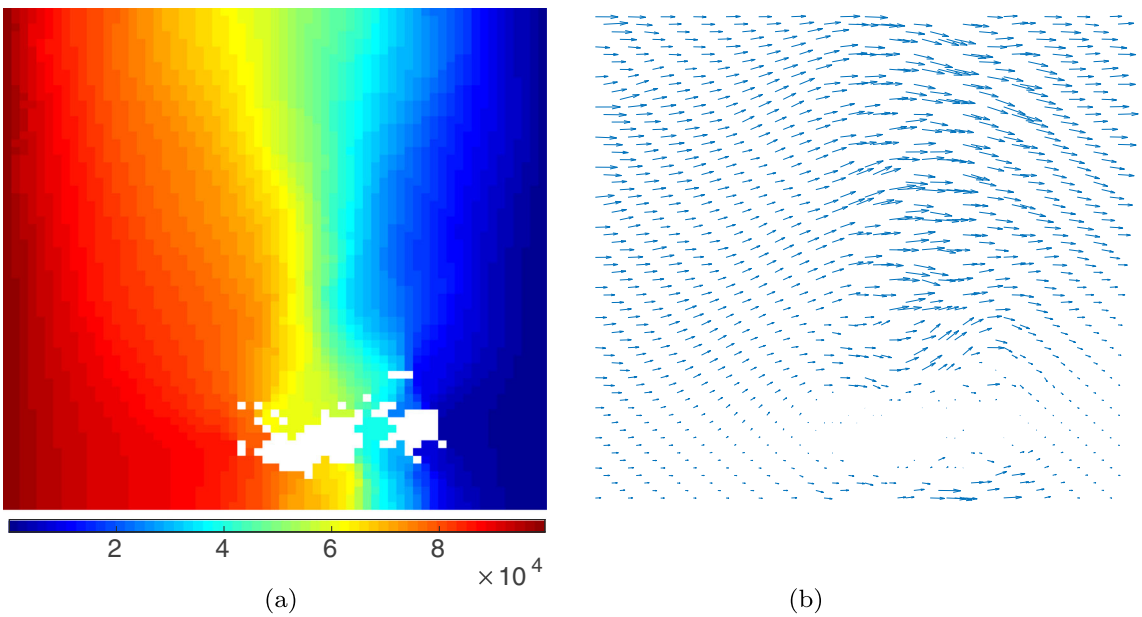

Fig. 7 Distribution of the fluid pressure (**a**) and superficial fluid velocity (**b**) in the partially-closed 1.02-mm fracture. *White spots* have zero aperture (contact between the fracture faces)

where the numerator is the average value of the absolute magnitude of the superficial fluid velocity; the denominator is the average value of the superficial fluid velocity's component in the direction parallel to the applied pressure differential. In our case, this is the direction of the x-axis. For a less tortuous (i.e., more unidirectional) flow, the value of T should be lower. For a perfectly unidirectional flow, e.g., in a fracture with smooth parallel walls, $T = 1$. For all other fractures, $T > 1$. The value of T depends on the aperture distribution of the fracture. For non-Newtonian fluids, it also depends on their rheological properties and the applied pressure gradient. In particular, shear-thinning fluids are known to produce less tortuous (more channelized) flows in rough-walled fractures than their Newtonian counterparts [17, 18].

3.1 Fracture flow of Bingham fluid

Simulations were performed with the following parameters of the regularized Bingham model: $\tau_Y = 10$ Pa, $\mu_{pl} = 0.01$ Pa · s, $n = 6$. Simulations were performed for pressure differential values from 10^3 to 10^7 Pa. Example results for the 1.7-mm and the partially-closed 1.02-mm fracture with 10^5 Pa pressure differential are shown in Figs. 6 and 7, respectively.

Tortuosity of the flow is greater for the partially-closed fracture than for the 1.7-*mm* fracture (Fig. 8). Tortuosity increases with the pressure differential for both fractures. The reason is that, at higher pressure differentials, the role of yield stress diminishes, i.e., the fluid behaves more and more like a Newtonian fluid. In the limit of an infinite pressure differential, the Bingham fluid would simply be a Newtonian fluid with the dynamic viscosity equal to μ_{pl} (cf. Fig. 1, $|\dot{\gamma}| \to \infty$).

On the contrary, as the pressure differential decreases, the shear-thinning behavior of the Bingham fluid plays more and more important role. As a result, the flow becomes more channelized [17]. Hence, the tortuosity decreases.

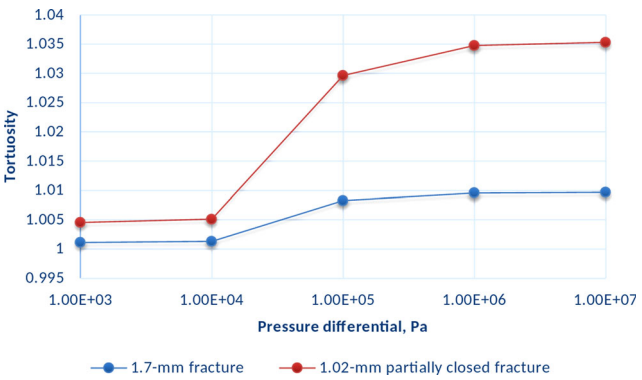

Fig. 8 Tortuosity as a function of pressure differential for regularized Bingham fluid

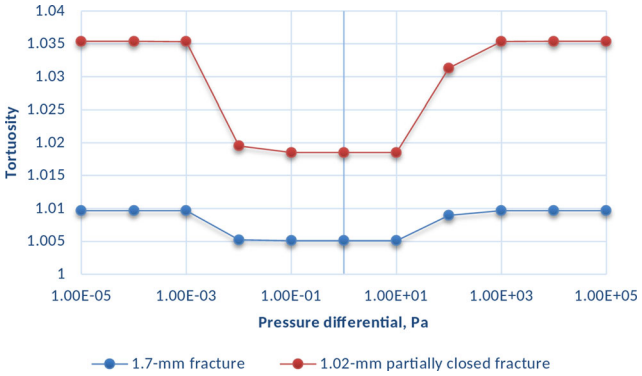

Fig. 9 Tortuosity as a function of pressure differential for shear-thinning truncated power-law fluid ($n = 0.6$)

3.2 Fracture flow of truncated power-law fluid

Simulations were performed for two truncated power-law fluids: a shear-thinning fluid and a shear-thickening fluid. The shear-thinning fluid had the following parameters: $n = 0.6$, $C = 0.005$ Pa · s^n, $\mu_0 = 0.5$ Pa ·s, $\mu_\infty = 0.001$ Pa · s. The shear-thickening fluid had the following parameters: $n = 1.4$, $C = 0.005$ Pa · s^n, $\mu_0 = 0.001$ Pa · s, $\mu_\infty = 0.01$ Pa · s. Simulations were performed for pressure differential values from 10^{-5} to 10^5 Pa.

The results for the shear thinning fluid are presented in Fig. 9. The tortuosity is lower at intermediate pressure differential values, and increases at very high or very low pressure differential values. This is due to the fluid becoming more like a Newtonian fluids at very high and very low shear rates, which was the very motivation for introducing this type of rheology. A shear-thinning fluids leads to more channelized flow than a Newtonian fluid, therefore, the tortuosity is lower at intermediate pressure differentials.

The opposite results are obtained with the shear-thickening truncated power-law fluid (Fig. 10). In this case, the flow is more tortuous at intermediate pressure

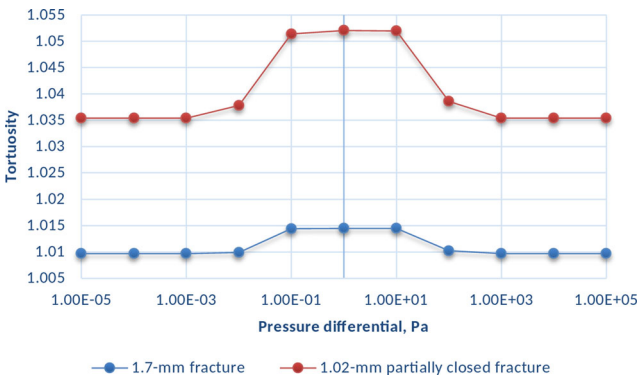

Fig. 10 Tortuosity as a function of pressure differential for shear-thickening truncated power-law fluid ($n = 1.4$)

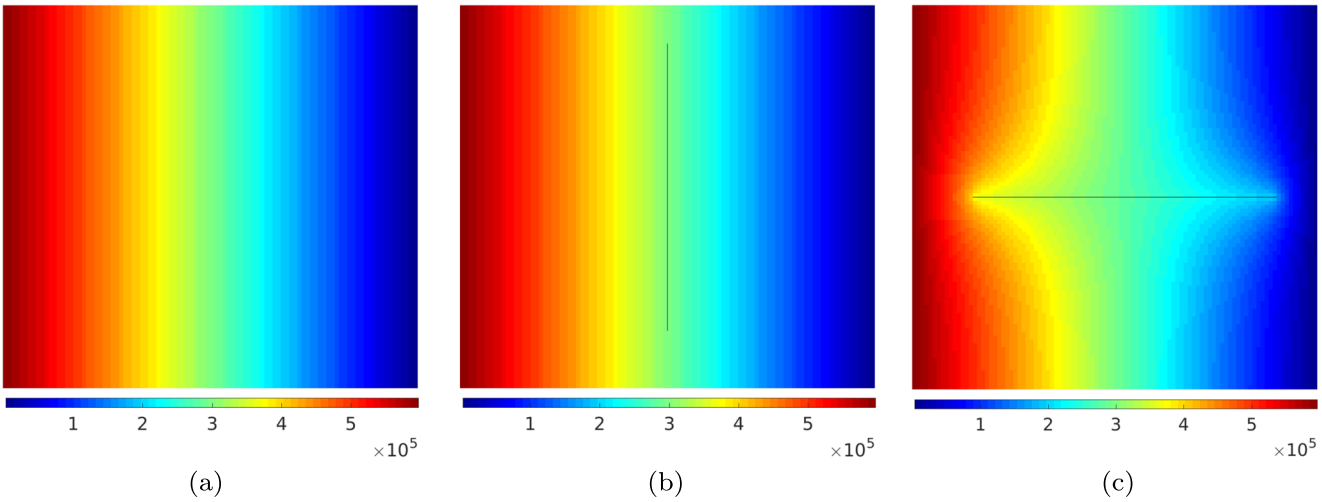

Fig. 11 Distribution of the fluid pressure in the simulations of fluid flow in the porous media with homogeneous permeability (**a**), a vertical fracture (**b**), and a horizontal fracture (**c**)

differential values. At very high and very low pressure differentials, the fluid is thinner as compared to the intermediate range. Therefore, the flow becomes more channelized (less tortuous) at very high and very low pressure differential values, where the fluid behaves close to a Newtonian fluid.

3.3 Truncated power-law fluid in porous media with a fracture

Simulations were performed for a shear-thinning truncated power-law fluid in porous media. Two models were assembled: one with homogeneous permeability (Fig. 11) and the other one with randomly generated heterogeneous permeability (Fig. 12). The fluid properties were as follows: $n = 0.6$, $C = 0.005$ Pa $\cdot$ s^n, $\mu_0 = 0.5$ Pa $\cdot$ s, $\mu_\infty = 0.001$ Pa $\cdot$ s. The dimensions of the computational domain were 20 m $\times$ 20 m $\times$ 5 m. The pressure differential applied between the left-hand boundary and the right-hand boundary was $6 \cdot 10^5$ Pa. A fracture was embedded in the domain. The objective of the simulations was to study how the existence and the orientation of the fracture would influence the flow in the porous media. The length of the fracture was 14 m; the aperture of the fracture was 1 mm. The fracture had the same aperture at all locations and thus was a smooth-walled fracture. For the homogeneous example (Fig. 11), the permeability of the porous media was set equal to 3 Darcy. For the heterogeneous example (Fig. 12), the permeability of the porous media was between $3 \cdot 10^{-2}$ mD and 3 Darcy, the average permeability being equal to 0.2613 Darcy.

As shown in Figs. 11 and 12, when the direction of the fracture was normal to the flow direction, the existence

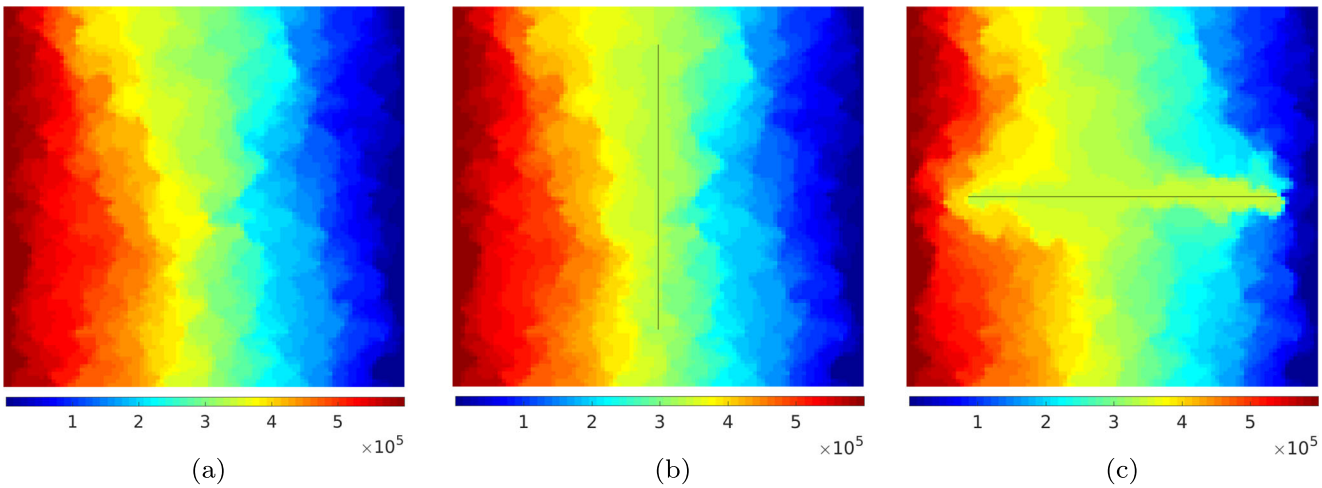

Fig. 12 Distribution of the fluid pressure in the simulations of fluid flow in the porous media with randomly generated heterogeneous permeability (**a**), a vertical fracture (**b**), and a horizontal fracture (**c**)

of the fracture virtually did not influence the flow, while when the direction of the fracture was along the flow direction, it affected the flow significantly. This was also reflected in the change of the flow rates. For the homogeneous example (Fig. 11), the flow rate without fracture was $8.4228 \cdot 10^{-3}$ m^3/s, the flow rate with a vertical fracture was the same ($8.4228 \cdot 10^{-3}$ m^3/s), while the flow rate with a horizontal fracture was $1.1708 \cdot 10^{-2}$ m^3/s. For the heterogeneous model (Fig. 12), the flow rates were $2.0005 \cdot 10^{-6}$ m^3/s, $2.1051 \cdot 10^{-6}$ m^3/s, and $4.9524 \cdot 10^{-6}$ m^3/s, respectively.

4 Conclusions and further work

Models for flow of Bingham fluid and truncated power-law fluid in porous media have been constructed. Closed-form solutions for flow between parallel plates were used for fracture flow. *Ad-hoc* equations were used for flow in porous media. The Bingham model was regularized by means of Papanastasiou-type regularization for flow in porous media, and by means of hyperbolic regularization for fracture flow. Taylor expansion of flow rate vs. pressure gradient was used to improve convergence at small pressure gradient values.

The models were tested on fracture flow in opened and partially-closed fractures. For a shear-thinning truncated power-law fluid, the flow becomes less tortuous (i.e., more channelized) at intermediate pressure gradient values. This is consistent with the well-known trend of shear-thinning fluids to result in channelization in rough-walled fractures. A shear-thickening truncated power-law fluid produces more tortuous flow at intermediate pressure gradient values. It produces more channelized flow at very high and very low pressure gradient values, where the truncated power-law fluid approached Newtonian rheology.

Regularized Bingham fluid produces more tortuous flow with increasing pressure differential. This is due to the diminishing role of yield stress at higher shear rates and, thus, at higher pressure differential values.

Simulations with porous media for truncated power-law fluid are also presented. The effect of the orientation of the fracture embedded in the porous media is investigated. An extension to the current fracture model will be required in order to handle more general and complicated fracture networks within porous media.

The truncated power-law and Bingham fluid rheologies used in this study only describe the correct relationship between the pressure drop and the flow rate in straight uniform conduits. These models are somewhat inadequate to describe the behavior of a non-Newtonian fluid in a porous medium, where the elastic nature of the fluid could be important (if the Deborah number is larger than 1). Therefore, Eqs. 27 and 28 can be valid for porous media, strictly speaking, only in a limiting case of low Deborah number. Implementation of visco-elastic fluid models for porous media and fractures in MRST should be the subject of further work.

More advanced rheological models might be required also to describe flow of polymer solutions/dispersions in porous media and small-aperture fractures. Pore throat clogging, polymer adsorption, and shear-induced polymer degradation are examples of phenomena that affect polymer flow in fractured and porous media. These phenomena should be accounted for in the model. The truncated power-law model used in this article can only serve as a first-order approximation for such fluids.

Only single-phase flow has been considered in this article. In multiphase flow, additional assumptions and/or closures would be required in the models. For instance, the threshold value of the pressure gradient in Eq. 9 for each phase must depend on the saturation since each phase only has a fraction of the pore (or fracture) volume at its disposal locally. Experiments may provide further important insights into multiphase flow of non-Newtonian fluids in fractured and porous media.

Acknowledgements The authors are grateful to two anonymous reviewers, whose comments have helped improve the manuscript. This publication has been produced with support from the KPN project "Controlled Fracturing for Increased Recovery." The authors acknowledge the following partners for their contributions: Lundin and the Research Council of Norway (244506/E30).

References

1. Alassi, H.T.: Modeling Reservoir Geomechanics Using Discrete Element Method: Application to Reservoir Monitoring, Ph.D. thesis, Norwegian University of Science and Technology (NTNU (2008)
2. Auradou, H., Boschan, A., Chertcoff, R., D'Angelo, M.V., Hulin, J.P., Ippolito, I.: Miscible transfer of solute in different model fractures: From random to multiscale wall roughness. Compt. Rendus Geosci. **342**(7), 644–652 (2010)
3. Auradou, H., Boschan, A., Chertcoff, R., Gabbanelli, S., Hulin, J., Ippolito, I.: Enhancement of velocity contrasts by shear-thinning solutions flowing in a rough fracture. J. Non-Newtonian Fluid Mech. **153**(1), 53–61 (2008)
4. Balhoff, M., Sanchez-Rivera, D., Kwok, A., Mehmani, Y., Prodanović, M.: Numerical algorithms for network modeling of yield stress and other non-newtonian fluids in porous media. Transp. Porous Media **93**(3), 363–379 (2012)
5. Bird, R., Armstrong, R., Hassager, O.: Dynamics of Polymer Liquids. Wiley, New York (1987)
6. Brown, S.R.: Fluid flow through rock joints: the effect of surface roughness. J. Geophys. Res. Solid Earth **92**(B2), 1337–1347 (1987)
7. Carreau, P.J.: Rheological equations from molecular network theories. Trans. Soc. Rheol. (1957-1977) **16**(1), 99–127 (1972)
8. Darby, R.: Chemical Engineering Fluid Mechanics, 2nd Edition. CRC Press, New York (2001)

9. Duda, A., Koza, Z., Matyka, M.: Hydraulic tortuosity in arbitrary porous media flow. Phys. Rev. E **84**(3), 036,319 (2011)
10. Frigaard, I., Nouar, C.: On the usage of viscosity regularisation methods for visco-plastic fluid flow computation. J. Non-Newtonian Fluid Mech. **127**(1), 1–26 (2005)
11. Hanssen, A.R.: Numerical Modelling of Bingham Fluid Flow and Particle Transport in a Rough-Walled Fracture,Master's thesis, Norwegian University of Science and Technology (NTNU) (2013)
12. Irgens, F.: Continuum mechanics Springer Berlin Heidelberg (2008)
13. Karimi-Fard, M., Durlofsky, L., Aziz, K., et. al: An efficient discrete-fracture model applicable for general-purpose reservoir simulators. SPE J. **9**(02), 227–236 (2004)
14. Koponen, A., Kataja, M., Timonen, J.: Tortuous flow in porous media. Phys. Rev. E. **54**(1), 406 (1996)
15. Lavrov, A.: Non-newtonian fluid flow in rough-walled fractures: A brief review. Rock Characterisation. Modelling and Engineering Design Methods 363 (2013)
16. Lavrov, A.: Numerical modeling of steady-state flow of a non-newtonian power-law fluid in a rough-walled fracture. Comput. Geotech. **50**, 101–109 (2013)
17. Lavrov, A.: Redirection and channelization of power-law fluid flow in a rough-walled fracture. Chem. Eng. Sci. **99**, 81–88 (2013)
18. Lavrov, A.: Radial flow of non-newtonian power-law fluid in a rough-walled fracture: effect of fluid rheology. Transp. Porous Media **105**(3), 559–570 (2014)
19. Lavrov, A.: Flow of truncated power-law fluid between parallel walls for hydraulic fracturing applications. J. Non-Newtonian Fluid Mech. **223**, 141–146 (2015)
20. Lavrov, A.: Lost circulation: Mechanisms and solutions. Elsevier (2016)
21. Lavrov, A., Larsen, I., Bauer, A.: Numerical modelling of extended leak-off test with a pre-existing fracture. Rock Mech. Rock. Eng. **49**(4), 1359–1368 (2016)
22. Lavrov, A., Larsen, I., Holt, R., Bauer, A., Pradhan, S., et al.: Hybrid FEM/DEM Simulation of Hydraulic Fracturing in Naturally-Fractured Reservoirs. In: 48Th US Rock Mechanics/Geomechanics Symposium. American Rock Mechanics Association (2014)
23. Lie, K.A., Krogstad, S., Ligaarden, I.S., Natvig, J.R., Nilsen, H.M., Skaflestad, B.: Open-source matlab implementation of consistent discretisations on complex grids. Comput. Geosci. **16**(2), 297–322 (2012)
24. Lipscomb, G., Denn, M.: Flow of bingham fluids in complex geometries. J. Non-Newtonian Fluid Mech. **14**, 337–346 (1984)
25. O'Donovan, E., Tanner, R.: Numerical study of the bingham squeeze film problem. J. Non-Newtonian Fluid Mech. **15**(1), 75–83 (1984)
26. Papanastasiou, T.C.: Flows of materials with yield. J. Rheol. **31**(5), 385–404 (1987)
27. Perkowska, M., Wrobel, M., Mishuris, G.: Universal hydrofracturing algorithm for shear-thinning fluids: Particle velocity based simulation. Comput. Geotech. **71**, 310–337 (2016)
28. Rossen, W., Gauglitz, P.: Percolation theory of creation and mobilization of foams in porous media. AIChE J **36**(8), 1176–1188 (1990)
29. Sandve, T., Berre, I., Nordbotten, J.M.: An efficient multi-point flux approximation method for discrete fracture–matrix simulations. J. Comput. Phys. **231**(9), 3784–3800 (2012)
30. Shah, C., Yortsos, Y.: Aspects of flow of power-law fluids in porous media. AIChE J. **41**(5), 1099–1112 (1995)
31. Sochi, T.: Modelling the flow of yield-stress fluids in porous media. Transp. Porous Media **85**(2), 489–503 (2010)
32. Talon, L., Auradou, H., Hansen, A.: Effective rheology of bingham fluids in a rough channel. Front. Phys. **2**, 24 (2014)
33. Valk, P., Economides, M.J.: Hydraulic Fracture Mechanics. Wiley, New York (1995)
34. White, F.M.: Fluid Mechanics. McGraw-Hill, New York (2003)
35. Wu, Y., Pruess, K., Witherspoon, P., et al.: Flow and displacement of bingham non-newtonian fluids in porous media. SPE Reserv. Eng. **7**(03), 369–376 (1992)
36. Zimmerman, R., Kumar, S., Bodvarsson, G.: Lubrication theory analysis of the permeability of rough-walled fractures. Int. J. Rock Mech. Min. Sci. Geomech. Abstr. **28**(4), 325–331 (1991)